Regional Arias Intensity Attenuation Relationship for Taiwan Considering V_{S30}

by Chyi-Tyi Lee, Bow-Shan Hsieh, Chih-Hsuan Sung, and Po-Shen Lin

Abstract The Arias intensity is a measure of earthquake intensity arrived at through the integration of a square of the acceleration time history. It has been demonstrated to be an effective predictor of earthquake damage potential in relation to short-period structures, liquefaction, and seismic slope stability, and has begun to be considered as a ground-motion measure suitable for use in probabilistic seismic hazard analysis (PSHA), as well as earthquake loss estimation. A new empirical Arias intensity attenuation relationship for shallow crustal earthquakes is developed where both fault type and a continuous site variable V_{S30} are considered. The relationship is based on a large number of strong-motion records (6570) from a wide range of earthquake magnitudes (3.9–7.6) from the Taiwan Strong Motion Instrument Program (TSMIP) network. Its functional form is modified from that of Travasarou *et al.* (2003), which is derived from a point-source model, and the coefficients are determined through nonlinear regression analyses using a mixed-effects model. The results show that the incorporation of V_{S30} can significantly reduce regression error. The Arias intensity value predicted in the present study is generally similar to that obtained by Travasarou *et al.* (2003), but is different in detail, being more suitable for usage in PSHA for a tectonically young orogenic belt like that in Taiwan or New Zealand.

Introduction

The Arias intensity (Arias, 1970) is an important measure of the strength of ground motion arrived at through the integration of the square of the acceleration time history. It is different from the peak ground acceleration (PGA), peak ground velocity (PGV), or individual ordinates of spectral acceleration (SA), which are also of interest in ground-motion attenuation relationship studies. The amplitude, frequency content, and duration of the ground motion are all incorporated in the intensity, and it is thus likely to be a more effective predictor of the earthquake damage potential. It correlates well with several commonly used demand measures of short-period structural performance, liquefaction (Kayen and Mitchell, 1997), and seismic slope stability (Wilson and Keefer, 1985; Harp and Wilson, 1995). In light of this utility, the Arias intensity has begun to be considered a ground-motion measure suitable for use in probabilistic seismic hazard analysis (PSHA) and earthquake loss estimation (Stafford *et al.*, 2009).

The attenuation relationship for the Arias intensity has been studied by various authors for different regions (e.g., Wilson and Keefer, 1985; Keefer and Wilson, 1989; Sabetta and Pugliese, 1996; Kayen and Mitchell, 1997; Paciello *et al.*, 2000; Travasarou *et al.*, 2003; Hwang *et al.*, 2004; Danciu and Tselentis, 2007; Stafford *et al.*, 2009). Taiwan is commonly recognized as a country with significant levels of seismic activity by worldwide standards, yet very few empirical ground-motion models have been derived for the area. This study takes a step toward remedying this situation by presenting new equations for predicting the Arias intensity of crustal earthquakes in Taiwan, for a wide range of magnitudes and distance values. In previous work, Travasarou *et al.* (2003) and Hwang *et al.* (2004) used the Chi-Chi dataset (Lee, Shin, *et al.*, 2001a; Lee, Cheng, *et al.*, 2001a) of Taiwan. However, their dataset is relatively small, and the continuous site parameter V_{S30} was not considered in these studies.

V_{S30} is the average shear-wave velocity in the upper 30 meters of a soil profile and is an important parameter for consideration in many earthquake ground-motion site-effect studies (Anderson *et al.*, 1996; BSSC, 1997a, b; Castro *et al.*, 1997; Park and Elrick, 1998). Borcherdt (1994) and Martin and Dobry (1994) recommended that structures be designed based on these properties. V_{S30} has been used by the Next Generation Attenuation of Ground Motions Project (NGA) of the Pacific Earthquake Engineering Research Center (PEER) in their ground-motion attenuation models (Abrahamson and Silva, 2008; Boore and Atkinson, 2008; Campbell and Bozorgnia, 2008; Chiou and Youngs, 2008; Idriss, 2008). It can be seen from this that V_{S30} has become very important in the field of ground-motion prediction and site-effect studies.

This study uses strong-motion data from the Taiwan Strong-Motion Instrument Program (TSMIP) to establish a new empirical Arias intensity attenuation relationship for shallow crustal earthquakes. The functional form of the attenuation model is modified from a version of the theoretical model proposed by Travasarou *et al.* (2003), by the addition of an alternative site term, V_{S30}. The maximum likelihood estimate (MLE) and mixed-effects model were used for regression. The goodness-of-fit of the median attenuation curve to the data was evaluated by analyses of inter-event and intra-event residuals and the residuals associated with site effect. The reduction of the standard deviation (sigma) for these terms will be discussed.

Regional Setting

Tectonic Environment

Taiwan is located at the convergent boundary between the Philippine Sea plate and the Eurasian plate. The Philippine Sea plate is moving northwest at a rate of about 7.3 cm/yr (Seno *et al.*, 1993) to 8 cm/yr (Yu *et al.*, 1997), while the Luzon arc at the leading edge of the Philippine Sea plate is colliding with the Eurasian plate in eastern Taiwan. In northeastern Taiwan, the Philippine Sea plate is subducting beneath the Eurasian plate. The strike of the Ryukyu trench near 121.5° E is oriented approximately northwest-southeast, but west of 125° E it rotates to follow a more east-west strike direction (see Fig. 1).

Tectonically, Taiwan is on the active collision zone between the Asiatic continent and the Luzon arc. The arc–continent collisions started in the late Miocene and are still vigorously taking place (Teng, 1990). The region is thus characterized by active crustal deformation (Bonilla, 1977; Yu *et al.*, 1997), frequent earthquakes (Tsai *et al.*, 1977), numerous typhoons, and a high erosion rate (Dadson *et al.*, 2003).

Site Geology

Geologically, the Central Range, which dominates the mountainous terrain of Taiwan, consists of a metamorphic complex and a Paleogene slate belt. The area is bordered by the Western Foothills, consisting of Neogene sedimentary formations, and the Eastern Coastal Range, also made up of Neogene sedimentary strata (Ho, 1975). The Longitudinal Valley, located between the Central Range and the Eastern Coastal Range, is a suture zone between the two plates.

The Taiwan region has a subtropical climate with an average annual precipitation of about 3000 mm and an average temperature of about 20° C. Physical and chemical weathering is significant and rapid, with slope wash and colluvium being widespread on hill slopes. Little hard rock exists at depths of less than 30 meters in this region.

There are Quaternary alluvial sediments, terrace deposits, basin deposits, and unconsolidated sedimentary strata in all geological provinces with a shear-wave velocity of less
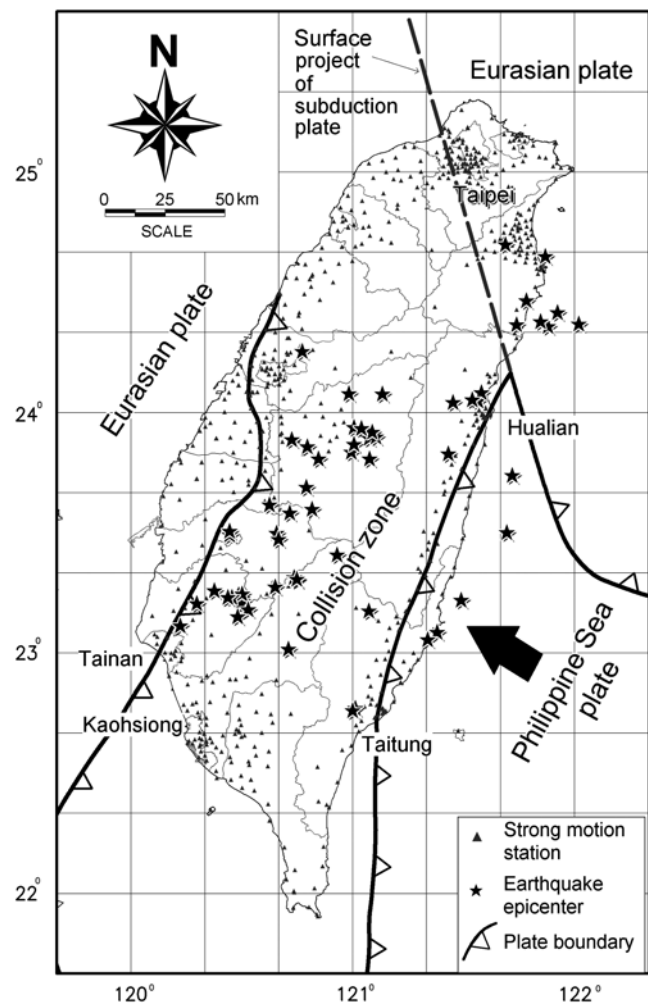
Figure 1. Plate architecture, locations of strong-motion stations, and earthquakes used in this study: a star indicates the epicenter of a shallow crustal earthquake, and a gray triangle shows the location of a strong-motion station.

than 760 m/s. The distribution of V_{S30} has been mapped by Lee and Tsai (2008) and is adopted in this study.

Data Acquisition and Processing

The strong-motion data used here were adopted from the Taiwan Next Generation Attenuation of Ground Motions Project (TNGA) database (see Data and Resources). Three major restrictions were considered in the data selection. First, earthquake events with less than ten records were not included. Second, strong-motion stations located on ridge tops were deleted. Third, records with insufficient supporting data for the focal mechanism or site condition were dropped. For example, the 11 stations marked as questionable in Lee, Cheng, *et al.* (2001a,b) were not included. The final selection included 6570 records from 62 crustal (hypocentral depth < 35 km) earthquakes (Table 1) and 657 stations. It is noted that the time, location, and depth of earthquakes in the TNGA database are directly from the Seismology Center of the Central Weather Bureau (CWB), Taiwan, and the moment

Table 1
Parameters of the Crustal Earthquakes in Taiwan Used in This Study

Number	Date (mm/dd/yy)	Time	Longitude	Latitude	Depth (km)	Magnitude (M_w)	Fault Type	Number of Records
1	12/13/93	09:23:30	120.776	24.256	22.45	4.32	RO	20
2	12/15/93	21:49:43	120.507	23.194	15.15	5.40	R	72
3	12/20/93	03:32:04	120.506	23.227	19.15	4.27	SS	24
4	12/21/93	03:14:28	120.509	23.216	14.45	4.35	R	18
5	12/22/93	16:22:20	120.499	23.208	16.95	4.49	SS	27
6	03/28/94	08:11:15	120.714	23.018	20.36	5.30	RO	60
7	04/06/94	01:12:11	120.448	23.494	18.65	4.91	SS	52
8	05/31/94	15:00:06	120.794	23.692	9.18	4.43	NO	23
9	06/05/94	01:09:30	121.787	24.468	5.13	6.30	NO	140
10	01/19/95	11:39:08	120.753	23.305	14.55	4.32	RO	31
11	02/26/95	08:08:18	121.384	23.088	22.3	4.74	RO	33
12	03/22/95	03:30:21	121.435	23.831	7.44	4.71	R	29
13	04/11/95	17:47:27	120.504	23.248	16.5	3.93	R	22
14	04/23/95	02:47:40	120.459	23.233	11.86	4.10	RO	26
15	04/23/95	02:57:52	120.437	23.233	9.8	4.17	SS	28
16	04/23/95	03:01:46	120.441	23.234	12.09	4.16	SS	34
17	05/01/95	14:50:45	121.569	24.052	12.99	4.76	RO	24
18	05/27/95	18:11:11	121.342	23.058	19.8	5.70	R	43
19	07/07/95	03:04:48	121.078	23.896	8.55	5.19	R	109
20	07/14/95	16:52:46	121.743	24.368	9.83	5.71	SS	90
21	09/28/95	17:58:05	120.449	23.509	11.93	4.34	SS	44
22	10/31/95	22:27:06	120.38	23.262	18.05	4.50	R	91
23	11/14/95	07:26:26	121.456	24.044	10.32	4.06	SS	24
24	04/07/96	16:55:36	120.67	23.475	4.44	4.57	R	27
25	10/19/96	19:16:05	120.532	23.183	13.6	4.06	R	35
26	11/16/96	00:22:43	120.300	23.208	20.2	4.13	RO	30
27	04/02/97	22:36:41	121.692	24.701	8.48	4.18	N	35
28	10/29/97	23:18:37	120.628	23.618	13.32	4.17	RO	26
29	01/18/98	19:56:51	121.015	22.773	3.34	5.22	SS	38
30	01/20/98	23:29:38	121.003	22.763	2.72	4.59	RO	26
31	07/17/98	04:51:14	120.660	23.500	6	5.66	R	39
32	09/20/99	17:47:15	120.799	23.860	6.76	7.62	R	372
33	09/20/99	17:57:14	121.010	23.940	8	5.90	R	256
34	09/20/99	18:03:40	120.850	23.810	8	6.20	N	212
35	09/20/1999	21:46:37	120.820	23.600	18	6.20	R	219
36	09/22/1999	00:14:40	121.080	23.810	10	6.20	RO	286
37	09/25/1999	23:52:49	121.010	23.870	16	6.30	R	259
38	02/15/00	21:33:18	120.740	23.316	14.71	5.14	RO	180
39	03/09/00	05:08:44	121.493	23.222	27.25	4.86	R	56
40	03/16/00	13:10:55	120.751	23.309	11.47	4.85	RO	133
41	06/10/00	18:23:29	121.109	23.901	13.7	6.07	R	331
42	06/19/00	21:56:24	121.092	23.920	25.65	4.91	RO	183
43	07/28/00	20:28:07	120.933	23.411	7.35	5.65	SS	173
44	09/01/00	09:24:38	121.138	24.080	7.69	4.77	SS	89
45	09/10/00	08:54:46	121.584	24.085	17.25	5.70	SS	157
46	12/10/00	19:30:44	120.226	23.116	12.02	4.95	SS	152
47	12/29/00	18:03:28	121.884	24.361	6.96	4.76	SS	63
48	01/11/01	08:36:59	120.987	24.081	21.05	4.56	N	113
49	02/18/01	20:25:10	120.719	23.585	15.65	4.37	SS	110
50	03/01/01	16:37:50	120.997	23.838	10.93	5.00	R	165
51	06/14/01	02:35:25	121.928	24.419	8.75	5.71	SS	189
52	06/19/01	05:16:15	121.077	23.177	6.58	5.00	N	98
53	06/30/01	04:07:37	121.543	24.055	22.2	4.51	R	96
54	09/17/01	22:44:44	120.654	23.276	6.83	4.82	R	71
55	11/04/01	08:45:35	121.043	23.936	7.48	4.44	R	77
56	02/12/02	03:27:25	121.723	23.741	35	5.52	RO	278
57	05/15/02	03:46:05	121.872	24.651	8.52	5.97	N	138
58	09/06/02	11:02:01	120.729	23.890	27.8	4.65	R	134
59	04/03/03	06:59:33	120.485	23.153	14.39	4.28	SS	70
60	06/09/03	01:52:50	122.023	24.370	24.4	5.58	SS	200
61	06/09/03	05:08:04	121.851	24.380	2.36	4.71	SS	66

Table 1 (*Continued*)

Number	Date (mm/dd/yy)	Time	Longitude	Latitude	Depth (km)	Magnitude (M_w)	Fault Type	Number of Records
62	06/10/03	08:40:32	121.699	23.504	35.05	5.71	R	324

Under Fault Type, SS is strike-slip, N is normal fault, NO is normal-oblique fault, R is reverse fault, and RO is reverse-oblique fault. The focal mechanism data are from Wu *et al.* (2008).

magnitude is adopted from Broadband Array in Taiwan for Seismology (BATS; Kao and Chen, 2000). Most of the magnitudes in Table 1 are from BATS, when there is no moment magnitude data, and then equation 1 in Lin and Lee (2008) was used to convert local magnitude from CWB to moment magnitude. All the fault types in Table 1 are adopted from Wu *et al.* (2008). The epicentral locations of earthquakes selected in this study and locations of the 657 stations are shown in Figure 1. The magnitude, distance, depth, and V_{S30} distribution of these earthquakes are shown in Figure 2. It can be seen that the dataset includes records from earthquakes having moment magnitudes ranging between 3.93 and 7.62, ground motions recorded at distances ranging between 0.3 km and 205 km, and V_{S30} ranging between 130 m/s and 1333 m/s.

Arias intensity, as defined by Arias (1970), is the total energy per unit weight stored by a set of simple oscillators evenly spaced in frequency. The Arias intensity for ground motion in the *x* direction (I_{xx}) may be written as

$$I_{xx} = \frac{\pi}{2g} \int_0^{T_d} a(t)^2 dt, \tag{1}$$

where $a(t)$ is the acceleration time history in the *x* direction, *g* is the acceleration due to gravity (both in m/s^2), and T_d is the total duration of ground motion in seconds. By definition, the Arias intensity is a second-order tensor, whose trace (i.e., $I_{xx} + I_{yy} + I_{zz}$) is an invariant. Consequently, all pairs of mutually perpendicular axes passing through a predefined origin have the same Arias intensity (m/s). Traditionally the Arias intensity is computed separately for each of the two perpendicular horizontal components of a recorded strong ground motion. Since most vertical strong-motion records contain relatively little of the total energy of shaking,
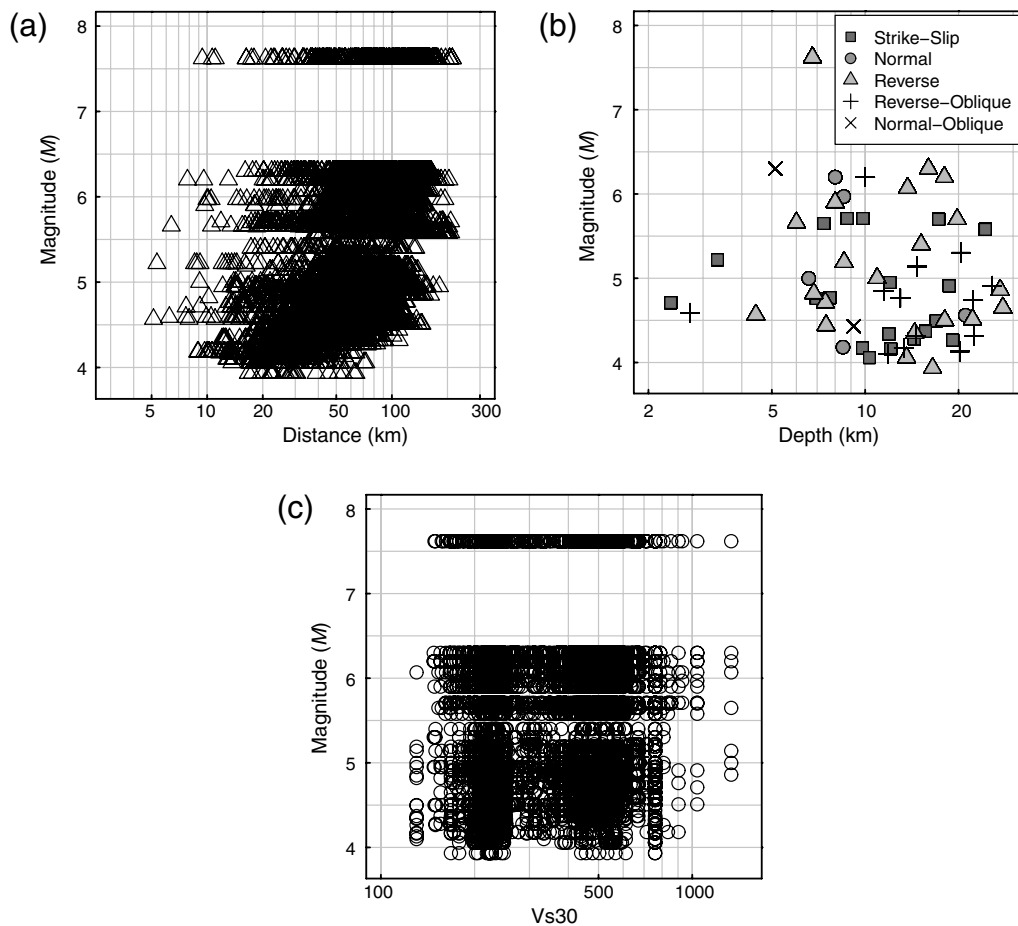
Figure 2.   Magnitude, distance, depth, and V_{S30} distribution of strong-motion data selected in the present study: (a) magnitude and distance distribution, (b) magnitude and depth distribution, and (c) magnitude and V_{S30} distribution.

they have been largely ignored in strong-motion engineering studies. In design practice, it would be desirable to predict the median of the average horizontal component during an earthquake scenario. This quantity $I_{xx} + I_{yy}$ is taken to be a constant (Travasarou *et al.*, 2003) and is easy to process from two mutually perpendicular strong-motion instruments. The proposed attenuation relationship estimates the parameter

$$I_a = \frac{I_{xx} + I_{yy}}{2}, \qquad (2)$$

where I_{xx} and I_{yy} are the Arias intensities computed from the two perpendicular horizontal components of the recorded strong ground motion.

V_{S30} is a key indicator of the site response dominating the ground-motion amplification. V_{S30} for each free-field strong-motion station in Taiwan has been evaluated and proposed by Lee and Tsai (2008). In the 2008 study, if measurement data are missing or a quality measurement record is not available, SPT-N values were used in the evaluation of a shear-wave velocity for soil and soft rock sites, or a value of 760 m/s was assigned to a rock site. During and after 2008, more measurements have become available, and the dataset is updated (see Data and Resources).

Attenuation Model and Regression Method

In the present study, we use a modification of the theoretically derived Arias intensity attenuation form from Travasarou *et al.* (2003). That form is based on the point-source model, with adjustments accounting for the finite-source effect and for nonlinear magnitude scaling. The form is further modified by adding an alternative site term V_{S30} as follows:

$$\ln I_a = c_1 + c_2(M - 6) + c_3 \ln(M/6) + c_4 \ln(\sqrt{R^2 + h^2})$$
$$+ c_5 \ln(V_{S30}/1130) + c_6 F_N + c_7 F_R + \eta + \varepsilon, \quad (3)$$

where M is the moment magnitude of an earthquake, R is the closest distance to the rupture plane (rupture distance) for large earthquakes and hypocentral distance for others in km, h is a fictitious hypocentral depth (in km) determined by the regression, V_{S30} is the average shear-wave velocity in the upper 30 meters of the soil profile, assuming that the V_{S30} of hard rock is equal to 1130 m/s (Chiou and Youngs, 2008), F_N and F_R are dummy variables for the fault types (both being 0 for strike-slip faults, 1 and 0, respectively, for normal faults, and 0 and 1, respectively, for reverse or reverse-oblique faults; rake angle less than 45 degrees or greater than 135 degrees is classified as a strike-slip fault), η is earthquake inter-event errors, and ε is intra-event errors.

The MLE and mixed-effects model are adopted in the nonlinear regression in equation (3) using the Taiwan crustal earthquake dataset mentioned previously. The processing was done using the nlme module in statistical software R (Pinheiro *et al.*, 2011).

Results and Evaluations

The attenuation relation for the Arias intensity is found using the mixed-effects model and MLE, using the Taiwan dataset. The median attenuation equation is

$$\ln I_a = 3.757 - 1.043(M - 6) + 18.077 \ln(M/6)$$
$$- 2.251 \ln(\sqrt{R^2 + 9.56^2}) - 1.042 \ln(V_{S30}/1130)$$
$$- 0.214 F_N + 0.220 F_R, \qquad (4)$$

where I_a is the arithmetic mean of the Arias intensities of two horizontal components in units m/s, and other variables are as previously defined. The inter-event standard deviation $\sigma_{\ln \eta}$ is 0.528, the intra-event standard deviation $\sigma_{\ln \varepsilon}$ is 0.842, and the total standard deviation σ_t, which is composed of $\sigma_{\ln \eta}$ and $\sigma_{\ln \varepsilon}$, is 0.994. The data used are 3.93–7.62 for earthquake magnitude, 0.3–205 km for rupture distance, 3–28 km for focal depth, and 130–1333 m/s for V_{S30}. These ranges may be referred to when predicting strong ground motion. Uncertainty should become larger if the model is used outside of these ranges, especially for a low V_{S30} value, because a nonlinear site effect is not considered in the present model.

The results show that different site conditions do produce different values of Arias intensity, as shown in Figure 3. Softer ground (with a lower V_{S30}) has a higher value of Arias intensity; the term for V_{S30} is negative and reflects this trend. Focal mechanisms also affect the result. Values for reverse faults are higher than those associated with strike-slip faults, and the values produced for strike-slip faults are higher than those for normal faults (Fig. 4). The minus coefficient for the term F_N means that motions from normal events are 0.214 smaller in natural log terms than from strike-slip events. The positive coefficient for the term F_R means that reverse events are 0.220 larger in natural log terms than for strike-slip events.

To confirm the results, we test the residuals obtained from the regression. Figure 5 shows the distribution of total residuals to the median of the Arias intensity attenuation relation. The good fit of the residuals to a log-normal distribution (Fig. 5a) and no trend of the residuals with distance (Fig. 5b) indicate that there is no bias exhibited in the regression results. There is a shift of the median values from zero; this is common for the total residuals in a mixed-effect model. If we examine the distribution of intra-event residuals, then the shift from zero will vanish. Distributions of inter-event residuals and intra-event residuals with distance and distributions of intra-event residuals with V_{S30} and those with earthquake magnitude are shown in Figure 6. There is no observable trend or change in the residuals with distance (Fig. 6a,b), with V_{S30} (Fig. 6c), or with earthquake magnitude (Fig. 6d). The negative value for the Chi-Chi event (Fig. 6a) probably represents the effect of surface rupture (Somerville, 2000; Kagawa *et al.*, 2004).

The goodness-of-fit of the median attenuation curves to the data is also shown by the actual data plot (Fig. 7).
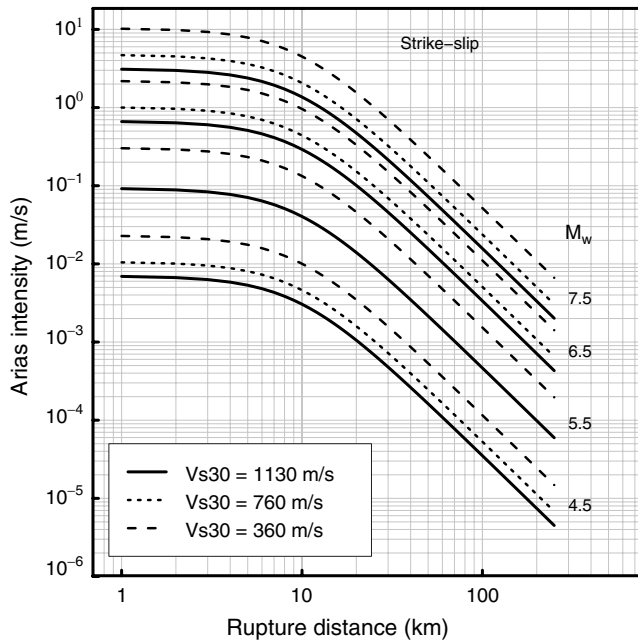
Figure 3. Arias intensity attenuation relationship for different magnitudes and V_{S30} for shallow crustal earthquakes.

Figure 7a shows the predicted values for the data from an *M* 7.62 reverse faulting earthquake (the Chi-Chi main shock). Figure 7b shows the predicted values for the data from the number 9 earthquake (see Table 1) with *M* 6.30 and an oblique-slip normal focal mechanism. Figure 7c shows the predicted values for the data from the number 57 earthquake with *M* 5.97 and a normal focal mechanism. Figure 7d shows the predicted values for the data from the number 29
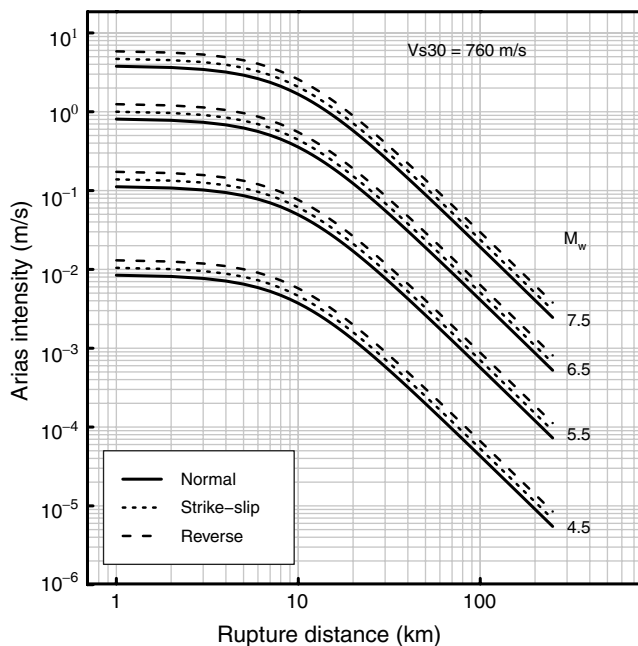
Figure 4. Arias intensity attenuation relationship for different magnitudes and fault styles for shallow crustal earthquakes.

earthquake with *M* 5.22 and a strike-slip earthquake focal mechanism. Figure 7e shows the predicted values for the data from the number 30 earthquake with *M* 4.59 and an oblique-slip reverse focal mechanism. Figure 7f shows the predicted values for the data from the number 25 earthquake with *M* 4.06 and a reverse faulting focal mechanism. The average V_{S30} value for all sites was adopted in plotting the previously mentioned attenuation curves.

Figure 8 compares distance scaling between this study and previous studies (Kayen and Mitchell, 1997; Travasarou et al., 2003; Hwang et al., 2004; Stafford et al., 2009; Foulser-Piggott and Stafford, 2011). The comparison reveals that although the value of the Arias intensity predicted in the present study is similar to that predicted by Travasarou et al. (2003) in general, the value predicted in the present study is slightly higher in the near distance (<30 km) and is lower in the far distance (>70 km). Hwang et al. (2004) obtained data for the main shock and three aftershocks of the Chi-Chi earthquake from stations in the footwall area and in the area away from the fault. Therefore, the data reflect only the relatively low nature of the ground motion of the Chi-Chi sequence. Kayen and Mitchell (1997) used a relatively small set of California earthquakes from Wilson (1993) and a relatively simple form for regression; these should not be overlooked in the comparison.

In a recent study, Stafford et al. (2009) used a New Zealand dataset and provided results for four different attenuation models, derived from the point-source model, with some different adjustments accounting for finite-source effects, nonlinear magnitude scaling, and so on. models one and two mainly consider linear magnitude scaling and magnitude saturation, whereas models three and four use different nonlinear magnitude scaling and distance saturation. The results for model one and model two of that study (Stafford et al., 2009) are similar to the results obtained in the present study for earthquakes with a magnitude larger than 6.5, but they differ for earthquake magnitudes smaller than 6.5, especially at the near distance. Results for model three and model four of that study (Stafford et al., 2009), however, are very similar to our results both in terms of prediction values and shape, as well as the slope of the attenuation curves. Because the present study uses a large amount of smaller earthquake magnitude data, our results should be more convincing for smaller earthquake magnitudes. Also, the results for Stafford et al. (2009) models three and four should be more persuasive. The great similarity between our results and the Stafford et al. (2009) models three and four results indicate the suitability of these attenuation equations for usage in PSHA for a tectonically young orogenic belt like Taiwan or New Zealand.

A brand-new study considering nonlinear site response and V_{S30} and using a subset of the PEER NGA database by Foulser-Piggott and Stafford (2011) indicates a similar result to our study, when rupture distance is between 20 km and 100 km (Fig. 8, Fig. 9f). The difference in the near field may be due to, primarily, the contrast of data from a young orogenic belt and the world-wide dataset. The use of more
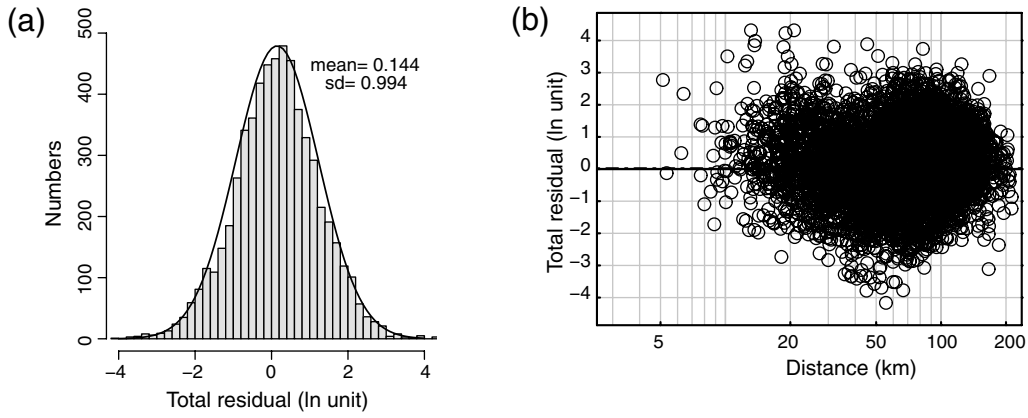
Figure 5.   Distribution of the total number of residuals to the median obtained with the Arias intensity attenuation equation: (a) histogram of total residuals and its fit to a normal distribution curve, and (b) distribution of total residuals with distance.

small earthquakes in our study may cause the larger difference in the smaller magnitudes, and the direct consideration of linear site response in our study may result in the overestimate of ground motion in the larger magnitudes in the near field. The difference in the far field may also be due to the difference in characteristics of the datasets, but the

use of more data in rupture distances larger than 100 km may also be the reason.

The pattern of the attenuation curves for different magnitudes can be visualized and compared (Fig. 9). Stafford *et al.* (2009) models three and four (Fig. 9e) are very similar to the results obtained in the present study (Fig. 9f). Travasarou,
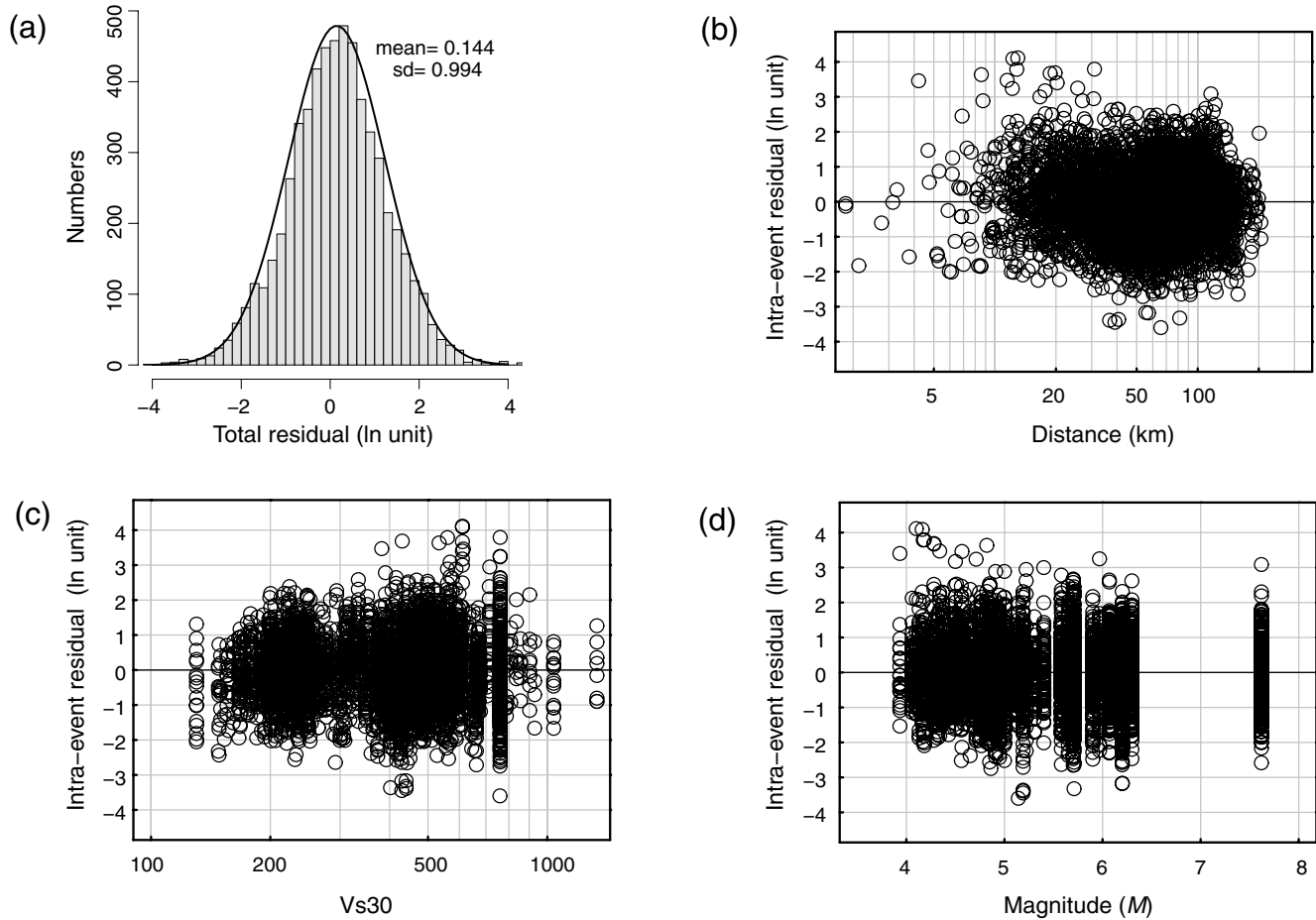
Figure 6.   Distribution of different residuals with different parameters obtained with the Arias intensity attenuation equation: (a) interresiduals with earthquake magnitude, (b) intraresiduals with distance, (c) intraresiduals with V$_{S30}$, and (d) intraresiduals with earthquake magnitude.
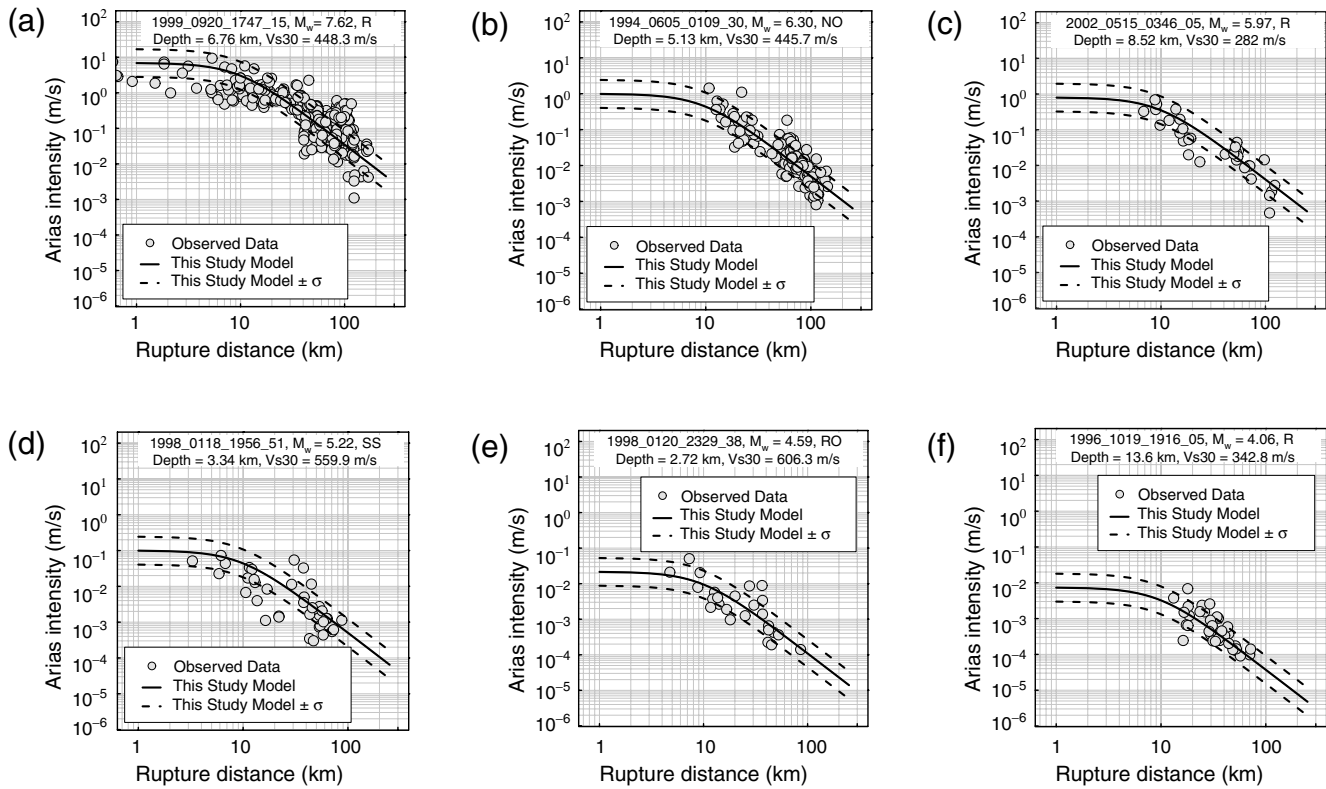
Figure 7. Fit of the median and one sigma Arias intensity attenuation curve obtained in this study to the data for (a) an *M* 7.62 reverse faulting earthquake, (b) an *M* 6.30 normal-oblique faulting earthquake, (c) an *M* 5.97 normal faulting earthquake, (d) an *M* 5.22 strike-slip earthquake, (e) an *M* 4.59 reverse-oblique faulting earthquake, and (f) an *M* 4.06 reverse faulting earthquake.

(2003) (Fig. 9c) is similar to Stafford *et al.* (2009) models three and four and the results obtained in the present study in pattern, but different in slope; the former being gentler. Travasarou (2003) used a world-wide dataset obtained from tectonically active regions. The steeper slope of Stafford *et al.* (2009) models three and four and our attenuation curves may be due to the crust in these two regions being weak, having low *Q* values, which is a common feature in a young orogenic belt.

A comparison of magnitude scaling between this study and previous studies (Kayen and Mitchell, 1997; Travasarou *et al.*, 2003; Hwang *et al.*, 2004; Bragato and Slejko, 2005; Stafford *et al.*, 2009; Foulser-Piggott and Stafford, 2011) is shown in Figure 10. Strike-slip faulting, site category D or $V_{S30} = 300$ m/s, and rupture distances of 1 km (Fig. 10a), 50 km (Fig. 10b), 100 km (Fig. 10c), and 150 km (Fig. 10d) are used for the comparison, except that in Kayen and Mitchell (1997) and in Hwang *et al.* (2004) rupture-line distances were used. The results reveal that model three of Stafford *et al.* (2009) is almost identical to the model of the present study, and Travasarou *et al.*, 2003 is also very similar to ours for the distance 1 km and 50 km cases. For the distance 100 km and 150 km cases, Travasarou *et al.* (2003) is similar only in trend, but it predicts a higher Arias intensity value than ours and model three of Stafford *et al.* (2009). This confirms the previously mentioned weak and low *Q* crust in Taiwan.

Among the 10 attenuation models, model three and model four of Stafford *et al.* (2009), Travasarou *et al.*, 2003, Foulser-Piggott and Stafford (2011), and this study show convex upward nonlinear magnitude scaling. Bragato and Slejko (2005) used data from earthquakes with magnitudes smaller than or equal to 6.3 to develop their attenuation model. It shows convex downward nonlinear magnitude scaling and leads to different trends beyond their data range. The other two models are of linear magnitude scaling.

A comparison of the regression errors shows the total standard deviation obtained in the present study ($\sigma_t = 0.994$) to be much smaller than that of Travasarou *et al.* (2003; $\sigma_t = 1.328$). It is also much smaller than that of Kayen and Mitchell (1997; $\sigma_t = 1.451$), that of Paciello *et al.* (2000; $\sigma_t = 1.247$), that of Hwang *et al.* (2004; $\sigma_t = 1.29$), that of Bragato and Slejko (2005; $\sigma_t = 1.586$), and that of Danciu and Tselentis (2007; $\sigma_t = 1.207$). It is comparable to or slightly smaller than that of Stafford *et al.* (2009; $\sigma_t = 1.0190 - 1.0324$ for soil sites, 1.1702–1.1821 for rock sites; see Table 2). Sabetta and Pugliese (1996) present a relatively smaller standard deviation ($\sigma_t = 0.914$), however, they only used a small dataset (95 records) with a narrow range of earthquake magnitudes (4.6–6.8) when developing their attenuation equation. Thus, we understand that the present study provides a good empirical attenuation relationship for the Arias intensity and the results should be useful.
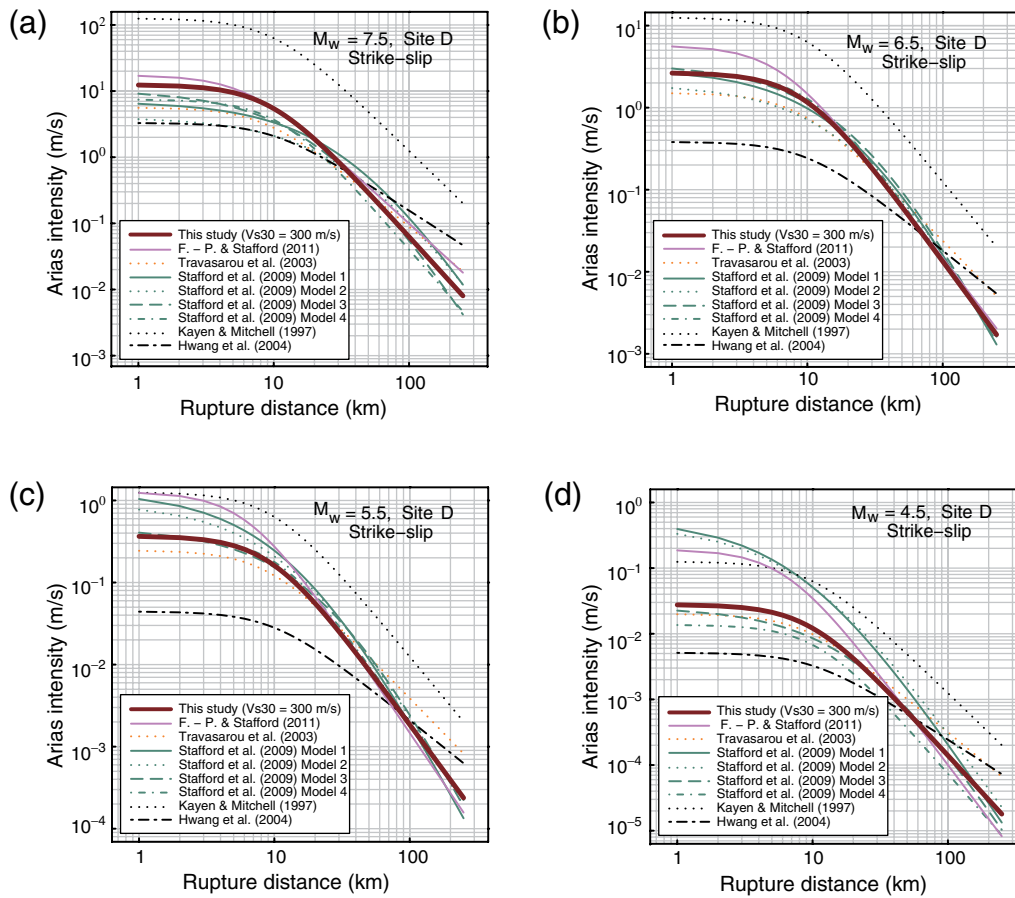
Figure 8. Comparison for distance scaling of attenuation equations between this study and previous studies. Please note that in this study, Travasarou *et al.* (2003), Stafford *et al.* (2009), and Foulser-Piggott and Stafford (2011) the rupture-plane distance was used, whereas in Kayen and Mitchell (1997) and in Hwang *et al.* (2004) the rupture-line distance was used. The color version of this figure is available only in the electronic edition.

Because the regression errors in the present study or in model three and model four of Stafford *et al.* (2009) are smaller than others, the nonlinear magnitude scaling they used should be better than linear magnitude scaling that was used by other previous studies (Kayen and Mitchell, 1997; Hwang *et al.*, 2004). We further select more strong-motion records from the TNGA database to validate the magnitude scaling problem at smaller magnitudes as plotted in Figure 10. The open circles in Figure 10 indicate that our nonlinear magnitude scaling model is also valid for earthquakes as small as about magnitude three, and the linear magnitude scaling models are not.

Model Development in the Present Study

To obtain as accurate a prediction of the ground-motion value as possible, it is desirable to compare the residual variance, as obtained from the regression analysis of different attenuation models, and to select an optimal attenuation form. During the study stage, we tested different attenuation models with the same dataset, then compared the residual variances. We also use Akaike Information Criterion (AIC)

to conform their statistical significance. AIC states that when a new term is added to the prediction equation, the maximum log likelihood must increase by one or more (Akaike, 1974).

During the first step of development, only the magnitude and distance terms were used in the model. The results showed that the residuals are dispersed with a total standard deviation of 1.229 and AIC equals 17,330.61. Next, site terms were added to the model using the site classes from Lee, Cheng, *et al.* (2001a,b). The results showed some improvement, giving a total standard deviation of 1.200. Third, we replaced the site classes with the V_{S30} from Lee and Tsai (2008). The results showed further improvement, with a total standard deviation of 1.161 and AIC equals 16,012.53. Fourth, we added a focal mechanism term to the model using focal mechanism data from BATS (Kao and Chen, 2000). The result showed further improvement with a total standard deviation of 1.108. Because some earthquakes lacked mechanism data, a strike-slip type was assumed for these earthquakes, and the total standard deviation is not persuasive. Lastly, the BATS data were replaced with focal mechanism data from Wu *et al.* (2008). The result showed great improvement, giving a total standard deviation of 0.994 and AIC equals 16,012.08
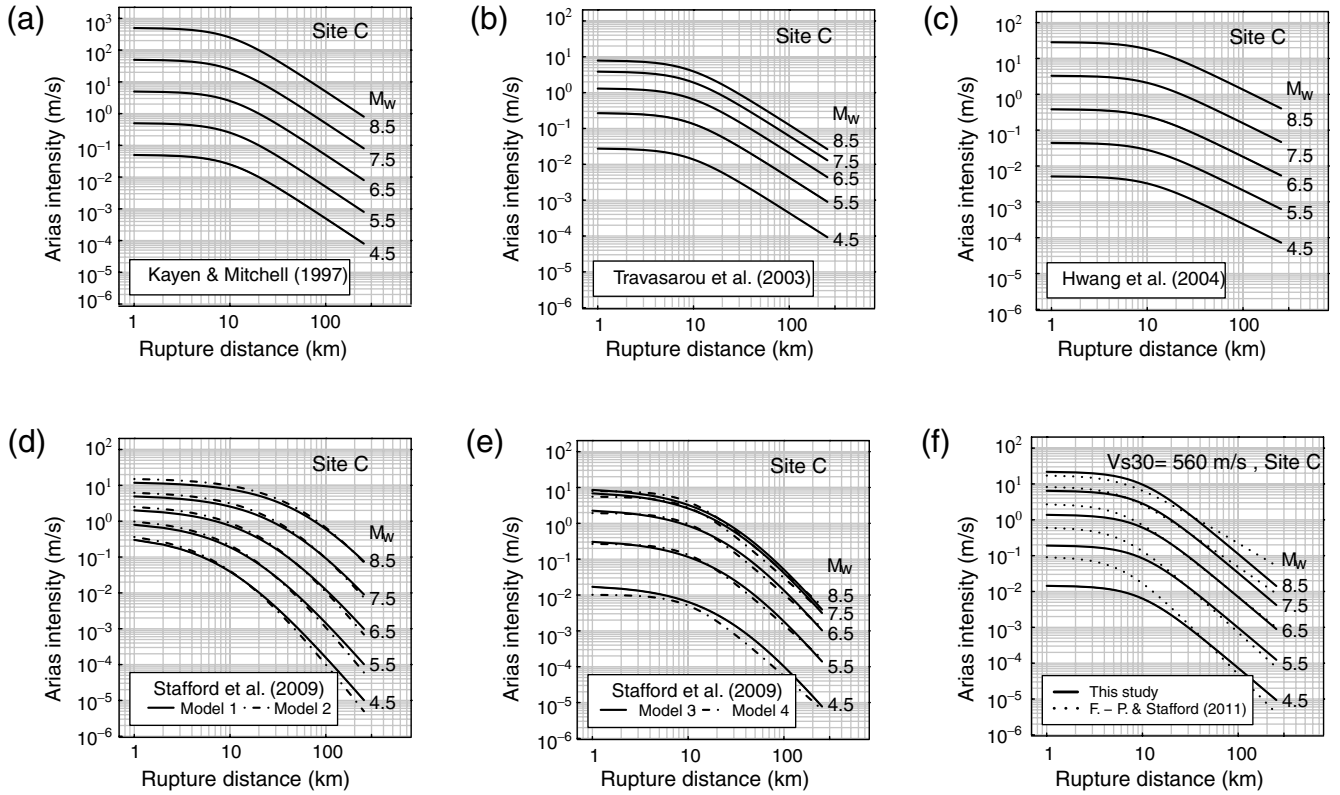
Figure 9.   Comparison of pattern and slopes of attenuation curves for various magnitudes from different studies.

(Table 3). Clearly, the inclusion of V_{S30} in the attenuation model is statistically significant and does reduce the regression error, thus resulting in a smaller sigma. The inclusion of the focal mechanism in the attenuation model is not statistically significant; however, it still has some physical meaning and reduces the regression error a little. Therefore, we reserve the use of focal mechanism terms in the attenuation model.

We also tested a fixed-effect model in the regression analysis, because it was commonly used in previous ground-motion attenuation studies in Taiwan. With the fixed-effect model, we obtain a total standard deviation of 1.080, slightly larger than that obtained by the mixed-effect model (0.994). The slope of the attenuation curves obtained from the fixed-effect model, which mixes data from different earthquake sources, is lower with lower values in the near distance and higher values in the far distance. The mixed-effect model could faithfully reflect the slope of an attenuation curve of an individual earthquake, and is deemed better at describing the attenuation relationship of Arias intensity. Therefore, the mixed-effect model is used throughout this study for the regression of the ground-motion attenuation relationship.

Intersite Residuals and Further Work

The residuals due to regression were decomposed into interevent (earthquake-to-earthquake) residuals and intraevent residuals. The intraevent residuals could be further decomposed into intersite (site-to-site) residuals and remain-

ing errors. There are three corresponding standard deviations: interevent standard deviation τ, intersite standard deviation σ_s, and the random one or the remainder σ_r (Chen and Tsai, 2002). Because these three terms are independent of each other, the total variance should be the sum of the three variances:

$$\sigma_t^2 = \tau^2 + \sigma_s^2 + \sigma_r^2. \qquad (5)$$

A mean and a standard deviation are calculated from the intraevent residuals at each station. This mean value varies from station to station. The standard deviation of these mean values from all stations is the intersite standard deviation σ_s, provided that data numbers at each station are large enough, and the standard deviation calculated from the remaining intraevent residuals is σ_r. In deriving σ_s, we select the stations that have at least 20 records for further refined study. A total of 68 stations and 1614 residuals were used to compute σ_s. The interevent standard deviation τ and the intraevent standard deviation σ were derived in the previous section. The five standard deviations are listed in Table 4. The five standard deviations for the case without considering V_{S30} are also listed for comparison.

We recall the interevent sigma and the intraevent sigma in Table 3. The reduction of total sigma by adding site terms is mainly due to the reduction of intraevent sigma, and the reduction of total sigma by adding focal mechanism terms is mainly due to the reduction of interevent sigma. Table 4
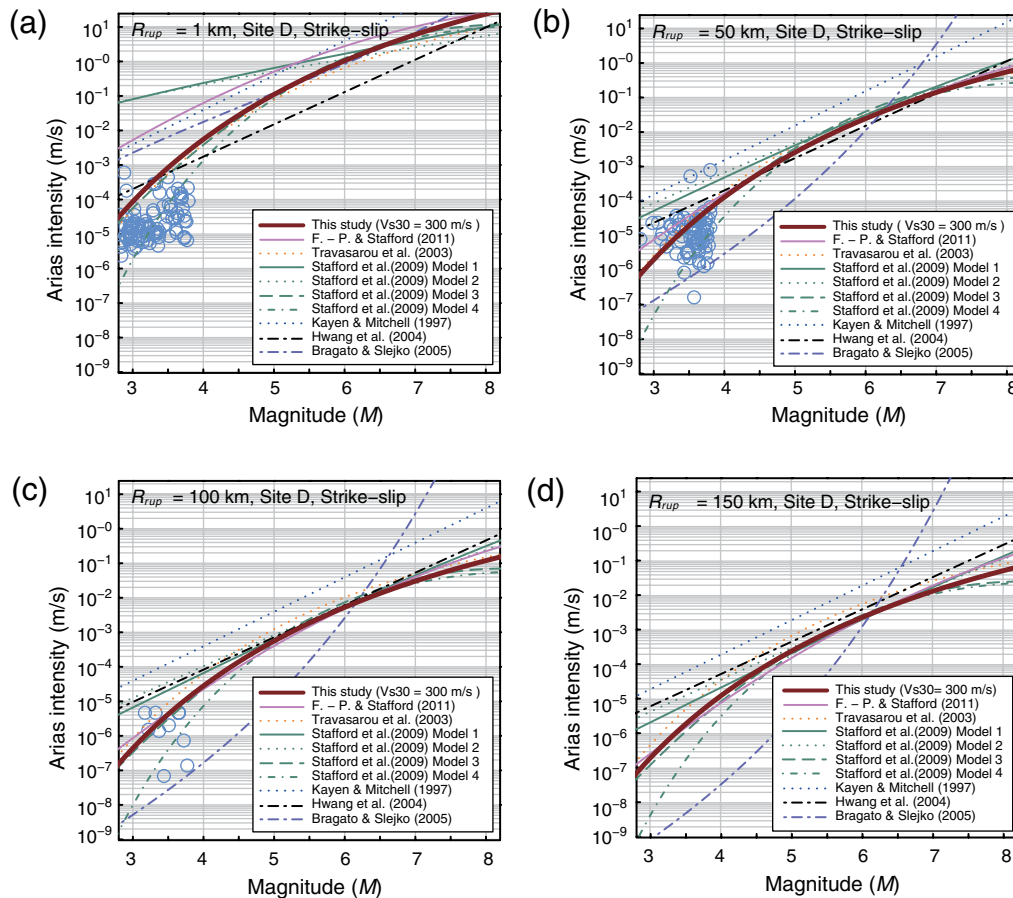
Figure 10. Comparison for magnitude scaling of attenuation equations between this study and previous studies. The open blue circles are smaller earthquakes beyond the present data set; these are used as a check. The color version of this figure is available only in the electronic edition.

again shows that the consideration of V_{S30} in the regression model largely reduces intraevent sigma, especially reducing the intersite sigma.

A single station sigma (Atkinson, 2006) σ_{ss} is the standard deviation of the total residuals at a specific station. We average the standard deviation of total residuals from the 68

Table 2
Standard Deviations from Different Attenuation Studies for Crustal Earthquakes

Arias Intensity Attenuation Study	Number of Earthquakes	Range of Magnitude	Number of Records	Total Sigma (σ_t)*
Sabetta and Pugliese (1996)	17	4.6 ~ 6.8	95	0.914
Kayen and Mitchell (1997)	8	6.1 ~ 7.9	1,080	1.451
Paciallo *et al.* (2000)	18	> 4.5	230	1.247
Travasarou *et al.* (2003)	75	4.7 ~ 7.6	1,208	1.328
Hwang *et al.* (2004)	4	6.2 ~ 7.7	1,602	1.290
Bragato and Slejko (2005)	240	2.5 ~ 6.3	4,570	1.460
Danciu and Tselentis (2007)	151	4.5 ~ 6.9	335	1.207
Stafford *et al.* (2009), Form 3	50	5.1 ~ 7.5	220	1.019[†]
				1.170[‡]
Stafford *et al.* (2009), Form 4	50	5.1 ~ 7.5	220	1.019[†]
				1.170[‡]
This study	62	3.9 ~ 7.6	6,570	0.994

*All the sigmas are in ln units.

[†]Soil site.

[‡]Rock site.

Moment magnitude, rupture distance, and Arias intensity obtained from the arithmetic mean of two horizontal components were used in all of the studies except Kayen and Mitchell (1997).

Table 3
Standard Deviations for Different Attenuation Models Obtained in This Study

Attenuation Model	Total Sigma (σ_t)	Interevent Sigma (τ)	Intraevent Sigma (σ)	AIC*
Only magnitude and distance terms	1.229	0.715	1.000	17330.61
Add site term (site class)	1.200	0.712	0.966	-
Add site term (V_{S30})	1.161	0.733	0.899	16012.53
Add focal mechanism term[†]	1.108	0.649	0.899	-
Add focal mechanism term[‡]	0.994	0.570	0.842	16012.08

*Akaike information criterion (Akaike, 1974).
[†]Focal mechanism data from BATS (Kao and Chen, 2000).
[‡]Focal mechanism data from Wu *et al.* (2008).

stations in this study and get a value of 0.897 in ln units, which is 10% lower than that of the total sigma. However, if we estimate the single station sigma by the variance decomposition method (Lin *et al.*, 2011), σ_{ss} is given by

$$\sigma_{ss}^2 = \sigma_t^2 - \sigma_s^2. \qquad (6)$$

Then, σ_{ss} is 0.868, which is 13% lower than the total sigma for Arias intensity when considering V_{S30}. The difference between the direct computation method mentioned previously and the use of equation (6) could be due to our dataset still not being large enough, or we should use the same dataset in computing σ_{ss} and σ_t, so that they can be compared.

Consideration of the path effect (Tsai, *et al.* 2006) and extraction of an interpath (path-to-path) standard deviation are also important. This process is currently under active study and will be presented in a separate paper. An attempt is made with these procedures to tailor sigma to a specific source–site configuration (Atkinson, 2006; Strasser *et al.*, 2009; Lin *et al.*, 2009). This is potentially the most promising approach to reducing sigma, with observed reductions of 40% to 50% in some cases. This reduction in sigma could reduce the hazard level in PSHA as discussed in Restrepo-Velez and Bommer (2003) and Bommer and Abrahamson (2006).

Nonlinear soil effects are recently considered in developing spectral attenuation relations (e.g., Abrahamson and Silva, 2008; Chiou and Youngs, 2008), because soil motion is deamplified under large strain (Bazzurro and Cornell, 2004). If nonlinear site effects are significant, we would observe an overprediction of the ground-motion level in the results. We reexamine Figure 7 to see if this fact exists. It tells that the overprediction feature is not obvious. However, when we examine a large earthquake (Chi-Chi) and near field data, then a slight overprediction feature is observed for soil sites. It is obvious that Arias intensity depicts nonlinear site effects and requires further study.

Conclusions and Recommendations

A new Arias intensity empirical attenuation relationship for shallow earthquakes, as well as the corresponding standard deviation for the ground-motion variability, is developed based on a large number of strong-motion data from the TNGA database. The results show that the mixed-effects model and MLE can effectively solve the regression problem for the treatment of uncertain earthquake magnitude and data heterogeneity. The inclusion of V_{S30} and the focal mechanism in the attenuation model can significantly reduce the total standard deviation. The nonlinear magnitude scaling form proposed by Travasarou *et al.* (2003) is suitable for fitting the Taiwan dataset for moment magnitudes between 3.9 and 7.6.

The median Arias intensity value predicted in the present study is similar to that predicted by Travasarou *et al.* (2003) in general, but slightly higher in the near distance (< 30 km) and lower in the far distance (> 70 km). However, the predicted value, shape, and slope of the attenuation curves are very similar to the results of functional models three and four by Stafford *et al.* (2009). The total standard deviation of the regression error obtained in this study is 0.994 (in ln units), which is smaller than that obtained in most other previous studies. The present Arias intensity attenuation relation is recommended for use in similar geological environments, especially for young orogenic belts like Taiwan and New Zealand.

Both the 2008 Wenchuan, China, earthquake (Li *et al.*, 2008) and the 1999 Chi-Chi, Taiwan, earthquake (Tsai and Huang, 2000) induced significant large ground shaking and severe damage on the hanging wall of the thrust fault. A slight overprediction of Arias intensity is observed for soil sites at near field of the Chi-Chi earthquake in the present study. Therefore, the hanging-wall effect and the nonlinear soil effects may be considered in the attenuation model in

Table 4
Standard Deviations of Different Terms Derived in This Study

	Total Sigma (σ_t)	Interevent Sigma (τ)	Intraevent Sigma (σ)	Intersite Sigma (σ_s)	Random Sigma (σ_r)
Considering V_{S30}	0.994	0.528	0.842	0.485	0.689
Without V_{S30}	1.158	0.532	1.028	0.629	0.841

further studies. Regression errors can be further minimized to make the results even more applicable in PSHA.

The attempt at effective extraction of the aleatory variability from the total residuals and tailoring sigma to a specific source–site configuration is actively proceeding. This is potentially the most promising approach to reducing sigma for reduction of the hazard level in PSHA and is worth pursuing in future studies.

Data and Resources

The strong-motion data used in the present study were adopted from the TNGA database (Lee *et al.*, 2006). This database contains strong-motion data collected from TSMIP from 1993 to 2003; this includes the main shock and five aftershocks of the Chi-Chi earthquake (Lee, Shin, *et al.*, 2001a,b). Base-line correction and filtering of the data were performed according to the standard procedures suggested by PEER (Darragh *et al.*, 2005).

The strong-motion data used in TNGA were purchased from CWB, Taiwan. They cannot be released to the public at present; however, the Bureau is now discussing its open data policy. Researchers need to wait for a while, or contact CWB directly.

The V_{S30} data used here are updated from Lee and Tsai (2008) and is available at http://gis.geo.ncu.edu.tw/Pub/Vs30.htm (last accessed November 2011).

Acknowledgments

References

Abrahamson, N. A., and W. Silva (2008). Summary of the Abrahamson & Silva NGA ground-motion relations, *Earthq. Spectra* **24,** 67–97, doi 10.1193/1.2924360.

Akaike, H. (1974). A new look at the statistical model identification, *IEEE Trans. Automat. Contr.* **19,** no. 6, 716–723, doi 10.1109/TAC.1974.1100705.

Anderson, J. G., Y. Lee, Y. Zeng, and S. Day (1996). Control of strong motion by the upper 30 meters, *Bull. Seismol. Soc. Am.* **86,** 1749–1759.

Arias, A. (1970). A measure of earthquake intensity, in *Seismic Design for Nuclear Power Plants*, R. J. Hansen (Editor), MIT Press, Cambridge, Massachusetts 438–483.

Atkinson, G. M. (2006). Single-station sigma, *Bull. Seismol. Soc. Am.* **96,** 446–455, doi 10.1785/0120050137.

Bazzurro, P., and C. A. Cornell (2004). Ground-motion amplification in nonlinear soil sites with uncertain properties, *Bull. Seismol. Soc. Am.* **94,** 2090–2109, doi 10.1785/0120030215.

Bommer, J. J., and N. A. Abrahamson (2006). Why do modern probabilistic seismic-hazard analyses often lead to increased hazard estimates? *Bull. Seismol. Soc. Am.* **96,** 1967–1977, doi 10.1785/0120060043.

Bonilla, M. G. (1977). Summary of Quaternary faulting and elevation changes in Taiwan, *Geol. Soc. China Mem.* **2,** 43–55.

Boore, D. M., and G. M. Atkinson (2008). Ground-motion prediction equations for the average horizontal component of PGA, PGV, and 5%-damped PSA at spectral periods between 0.01 s and 10.0 s, *Earthq. Spectra* **24,** 99–138.

Borcherdt, R. D. (1994). Estimates of site-dependent response spectra for design (methodology and justification), *Earthq. Spectra* **10,** 617–653, doi 10.1193/1.1585791.

Bragato, P. L., and D. Slejko (2005). Empirical ground-motion attenuation relations for the eastern Alps in the magnitude range 2.5–6.3, *Bull. Seismol. Soc. Am.* **95,** 252–276, doi 10.1785/0120030231.

Building Seismic Safety Council (BSSC) (1997a). NEHPR recommended provisions for seismic regulations for new buildings and other structures, Part 1: Provisions (FEMA 302), National Institute of Building Sciences, developed for the Federal Emergency Management Agency, Washington D. C., 336 p.

Building Seismic Safety Council (BSSC) (1997b). NEHPR recommended provisions for seismic regulations for new buildings and other structures, Part 2: Commentary (FEMA 303), National Institute of Building Sciences, developed for the Federal Emergency Management Agency, Washington D. C., 336 pp.

Campbell, K. W., and Y. Bozorgnia (2008). NGA ground motion model for the geometric mean horizontal component of PGA, PGV, PGD and 5% damped linear elastic response spectra for periods ranging from 0.01 to 10 s, *Earthq. Spectra* **24,** 139–171, doi 10.1193/1.2857546.

Castro, R. R., M. Mucciarelli, F. Pacor, and C. Petrungaro (1997). *S*-wave site-response estimates using horizontal-to-vertical spectral rations, *Bull. Seismol. Soc. Am.* **87,** 256–260.

Chen, Y. H., and C. P. Tsai (2002). A new method of estimation of the attenuation relationship with variance components, *Bull. Seismol. Soc. Am.* **92,** 1984–1991, doi 10.1785/0120010205.

Chiou, B. S., and R. R. Youngs (2008). An NGA model for the average horizontal component of peak ground motion and response spectra, *Earthq. Spectra* **24,** 173–215, doi 10.1193/1.2894832.

Dadson, S. J., N. Hovious, H. Chen, B. W. Dade, S. D. Willett, J. C. Hu, M. J. Horng, M. C. Chen, C. P. Stark, D. Lague, and J. C. Lin (2003). Links between erosion, runoff variability, and seismicity in the Taiwan orogen, *Nature* **426,** 648–651, doi 10.1038/nature02150.

Danciu, L., and G. A. Tselentis (2007). Engineering ground-motion parameters attenuation relationships for Greece, *Bull. Seismol. Soc. Am.* **97,** 162–183, doi 10.1785/0120050087.

Darragh, B., W. Silva, and N. Gregor (2005). Strong motion record processing for the PEER center, http://www.cosmos-eq.org:16080/events/wkshop_records_processing/papers/Darragh_Silva_Gregor_Paper.pdf (last accessed November 2011).

Foulser-Piggott, R., and P. J. Stafford (2011). A predictive model for Arias intensity at multiple sites and consideration of spatial correlations, *Earthq Eng. Struct. Dynam.* doi 10.1002/eqe.1137.

Harp, E. L., and R. C. Wilson (1995). Shaking intensity thresholds for rock falls and slides: Evidence from 1987 Whittier Narrows and Superstition Hills earthquake strong-motion records, *Bull. Seismol. Soc. Am.* **85,** 1739–1757.

Ho, C. S. (1975). *An introduction to the geology of Taiwan, explanatory text of the geologic map of Taiwan*, Ministry of Economic Affairs, ROC, 312 p.

Hwang, H., C. K. Lin, Y. T. Yeh, S. N. Cheng, and K. C. Chen (2004). Attenuation relations of Arias intensity based on the Chi-Chi Taiwan earthquake data, *Soil Dynam. Earthq. Eng.* **24,** 509–517.

Idriss, I. M. (2008). An NGA empirical model for estimating the horizontal spectral values generated by shallow crustal earthquakes, *Earthq. Spectra* **24,** 217–242, doi 10.1193/1.2924362.

Kao, H., and W. P. Chen (2000). The Chi-Chi earthquake sequence: Active, out-of-sequence thrust faulting in Taiwan, *Science* **288,** 2346–2349, doi 10.1126/science.288.5475.2346.

Kagawa, T., K. Irikura, and P. G. Somerville (2004). Differences in ground motion and fault rupture process between the surface and buried rupture earthquakes, *Earth Planets Space* **56,** 3–14.

Kayen, R. E., and J. K. Mitchell (1997). Assessment of liquefaction potential during earthquakes by Arias intensity, *J. Geotech. Geoenviron. Eng.* **123,** 1162–1174.

Keefer, D. K., and R. C. Wilson (1989). Predicting earthquake-induced landslides, with emphasis on arid and semi-arid environments, in *Landslides in a semi-arid environment with emphasis on the inland valleys of southern California*, P. M. Sadler and D. M. Morton (Editors), Inland Geological Society of Southern California Publications **2**, 118–149.

Lee, C. T., and B. R. Tsai (2008). Mapping V_{S30} in Taiwan, *Terr. Atmos. Ocean. Sci.* **19**, 671–682, doi 10.3319/TAO.2008.19.6.671(PT).

Lee, C. T., H. C. Chiu, P. S. Lin, and C. T. Cheng (2006). Research on establishment and maintenance of strong-motion database and development of user platform, Sinotech Engineering Consultants, Inc., Taiwan, 83 p.

Lee, C. T., C. T. Cheng, C. W. Liao, and Y. B. Tsai (2001a). Site classification of Taiwan free-field strong-motion stations, *Bull. Seismol. Soc. Am.* **91**, 1283–1297, doi 10.1785/0120000736.

Lee, C. T., C. T. Cheng, C. W. Liao, and Y. B. Tsai (2001b). Data file from "Site classification of Taiwan free-field strong-motion stations", *Bull. Seismol. Soc. Am.* **91**, 1386, doi 10.1785/0120000753.

Lee, W. H. K., T. C. Shin, K. W. Kuo, K. C. Chen, and C. F. Wu (2001a). CWB free-field strong-motion data from the 21 September Chi-Chi, Taiwan earthquake, *Bull. Seismol. Soc. Am.* **91**, 1370–1376, doi 10.1785/0120000744.

Lee, W. H. K., T. C. Shin, K. W. Kuo, K. C. Chen, and C. F. Wu (2001b). Data files from "CWB free-field strong-motion data from the 21 September Chi-Chi, Taiwan, earthquake", *Bull. Seismol. Soc. Am.* **91**, 1390, doi 10.1785/0120000756.

Li, X., Z. Zhou, H. Yu, R. Wen, D. Lu, M. Huang, Y. Zhou, and J. Cu (2008). Strong motion observations and recordings from the great Wenchuan Earthquake, *Earthq. Eng. Eng. Vib.* **7**, 235–246.

Lin, P. S., and C. T. Lee (2008). Ground-motion attenuation relationships for subduction-zone earthquakes in northeastern Taiwan, *Bull. Seismol. Soc. Am.* **98**, 220–240, doi 10.1785/0120060002.

Lin, P. S., C. T. Lee, N. Abrahamson, and B. Chiou (2009). Repeatable path effects on the standard deviation for empirical ground motion models, in *Proc. of the Next Generation of Research on Earthquake-induced Landslides—an International Conference in Commemoration of 10th Anniversary of the Chi-Chi Earthquake*, National Central University, Jhongli, Taiwan, 21–26 September 2009.

Lin, P. S., B. Chiou, N. Abrahamson, M. Walling, C. T. Lee, and C. T. Cheng (2011). Repeatable source, site, and path effects on the standard deviation for empirical ground motion prediction models, *Bull. Seismol. Soc. Am.* **101**, no. 5, 2251–2295, doi 10.1785/0120090312.

Martin, G. R., and R. Dobry (1994). Earthquake site response and seismic code provisions, *NCEER Bull.* **8**, 1–6.

Paciello, A., D. Rinaldis, and R. Romeo (2000). Incorporating ground motion parameters related to earthquake damage into seismic hazard analysis, in *Proc. of the Sixth International Conf. on Seismic Zonation: Managing Earthquake Risk in the 21st Century*, Earthquake Engineering Research Institute, Oakland, California, November 2000.

Park, S., and S. Elrick (1998). Predictions of shear-wave velocities in southern California using surface geology, *Bull. Seismol. Soc. Am.* **88**, 677–685.

Pinheiro, J., D. Bates, S. DebRoy, D. Sarkar , and The R Core Team (2011). nlme: Linear and nonlinear mixed effects models, R package version 3.1-102.

Restrepo-Velez, L. F., and J. J. Bommer (2003). An exploration of the nature of the scatter in ground motion prediction equations and the implications for seismic hazard assessment, *J. Earthq. Eng.* **7**, 171–199.

Sabetta, F., and A. Pugliese (1996). Estimation of response spectra and simulation of nonstationary earthquake ground motions, *Bull. Seismol. Soc. Am.* **86**, 337–352.

Seno, T., S. Stein, and A. E. Gripp (1993). A model for the motion of the Philippine Sea plate consistent with NUVEL-1 and geological data, *J. Geophys. Res.* **98**, 941–948.

Somerville, P. G. (2000). Magnitude scaling of near fault ground motions, *Earthq. Eng. Eng. Seismol.* **2**, no. 2, 15–24.

Stafford, P. J., J. B. Berrill, and J. R. Pettinga (2009). New predictive equations for Arias intensity from crustal earthquakes in New Zealand, *J. seismol.* **13**, 31–52.

Strasser, F. O., N. A. Abrahamson, and J. J. Bommer (2009). Sigma: Issues, insights, and challenges, *Seismol. Res. Lett.* **80**, 40–56, doi 10.1785/gssrl.80.1.40.

Teng, L. S. (1990). Geotectonic evolution of late Cenozoic arc-continent collision in Taiwan, *Tectonophysics* **183**, 57–76.

Travasarou, T., J. D. Bray, and N. A. Abrahamson (2003). Empirical attenuation relationship for Arias intensity, *Earthq. Eng. Sturct. Dynam.* **32**, 1133–1155, doi 10.1002/eqe.270.

Tsai, C. P., Y. H. Chen, and C. H. Liu (2006). The path effect in ground-motion variability: An application of the variance-components technique, *Bull. Seismol. Soc. Am.* **96**, 1170–1176, doi 10.1785/0120050155.

Tsai, Y. B., and M. W. Huang (2000). Strong ground motion characteristics of the Chi-Chi, Taiwan earthquake of September 21, 1999, *Earthq. Eng. Eng. Seismol.* **2**, 1–21.

Tsai, Y. B., T. L. Teng, J. M. Chiu, and H. L. Liu (1977). Tectonic implications of the seismicity in the Taiwan region, *Geol. Soc. China Mem.* **2**, 13–41.

Wilson, R. C. (1993). Relation of Arias intensity to magnitude and distance in Carifornia, *U. S. Geol. Surv. Open-File Rept. 93-556*, 38–42.

Wilson, R. C., and D. K. Keefer (1985). Predicting areal limits of earthquake-induced landsliding, in *Evaluating Earthquake Hazards in the Los Angeles Regine*, *U. S. Geol. Surv. Profess. Pap. 1360*, 317–345.

Wu, Y. M., L. Zhao, C. H. Chang, and Y. J. Hsu (2008). Focal mechanism determination in Taiwan by genetic algorithm, *Bull. Seismol. Soc. Am.* **98**, 651–661, doi 10.1785/0120070115.

Yu, S. B., H. Y. Chen, and L. C. Kuo (1997). Velocity field of GPS stations in the Taiwan area, *Tectonophysics* **274**, 41–59, doi 10.1016/S0040-1951(96)00297-1.

Graduate Institute of Applied Geology
National Central University
No. 300 Jhongda Rd
Jhongli City, Taoyuan 32001
Taiwan
ct@ncu.edu.tw
bowmei@gis.geo.ncu.edu.tw
karen@gis.geo.ncu.edu.tw
person@gis.geo.ncu.edu.tw